

Article

Digital Twins for scFv Production in *Escherichia coli*

Heribert Helgers, Alina Hengelbrock , Axel Schmidt , Florian Lukas Vetter, Alex Juckers  and Jochen Strube *

Institute for Separation and Process Technology, Clausthal University of Technology, Leibnizstr. 15, 38678 Clausthal-Zellerfeld, Germany; helgers@itv.tu-clausthal.de (H.H.); hengelbrock@itv.tu-clausthal.de (A.H.); schmidt@itv.tu-clausthal.de (A.S.); vetter@itv.tu-clausthal.de (F.L.V.); juckers@itv.tu-clausthal.de (A.J.)

* Correspondence: strube@itv.tu-clausthal.de

Abstract: Quality-by-Design (QbD) is demanded by regulatory authorities in biopharmaceutical production. Within the QbD frame advanced process control (APC), facilitated through process analytical technology (PAT) and digital twins (DT), plays an increasingly important role as it can help to assure to stay within the predefined proven acceptable range (PAR). This ensures high product quality, minimizes failure and is an important step towards a real-time-release testing (RTRT) that could help to accelerate time-to-market of drug substances, which is becoming even more important in light of dynamical pandemic situations. The approach is exemplified on scFv manufacturing in *Escherichia coli*. Simulation results from digital twins are compared to experimental data and found to be accurate and precise. Harvest is achieved by tangential flow filtration followed by product release through high pressure homogenization and subsequent clarification by tangential flow filtration. Digital twins of the membrane processes show that shear rate and transmembrane pressure are significant process parameters, which is in line with experimental data. Optimized settings were applied to 0.3 bar and a shear rate of $11,000 \text{ s}^{-1}$. Productivity of chromatography steps were 5.3 g/L/d (Protein L) and 2167 g/L/d (CEX) and the final product concentration was 8 g/L . Based on digital twin results, an optimized process schedule was developed that decreased purification time to one working day, which is a factor-two reduction compared to the conventional process schedule. This work presents the basis for future studies on advanced process control and automation for biologics production in microbials in regulated industries.

Keywords: digital twin (DT); advanced process control (APC); quality-by-design (QbD); process analytical technology (PAT); real-time-release testing (RTRT); *Escherichia coli* (*E. coli*); single-chain fragment variable (scFv)



Citation: Helgers, H.; Hengelbrock, A.; Schmidt, A.; Vetter, F.L.; Juckers, A.; Strube, J. Digital Twins for scFv Production in *Escherichia coli*. *Processes* **2022**, *10*, 809. <https://doi.org/10.3390/pr10050809>

Academic Editor: Alina Pyka-Pajak

Received: 24 March 2022

Accepted: 11 April 2022

Published: 20 April 2022

Publisher's Note: MDPI stays neutral with regard to jurisdictional claims in published maps and institutional affiliations.



Copyright: © 2022 by the authors. Licensee MDPI, Basel, Switzerland. This article is an open access article distributed under the terms and conditions of the Creative Commons Attribution (CC BY) license (<https://creativecommons.org/licenses/by/4.0/>).

1. Introduction

Among prokaryotic organisms for the production of pharmaceutically active and commercially relevant proteins, *Escherichia coli* (*E. coli*) is the most widely used [1]. Because the bacterium has been extensively studied, has high growth rates, can grow to high cell densities, and grows on inexpensive, chemically defined media, it is a well-suited production organism [2,3]. A major drawback is that *E. coli* is not capable of post-translational modifications, such as glycosylation. However, non-glycosylated therapeutic proteins, such as insulin, various growth factors, interferons, and antibody fragments can be efficiently produced with *E. coli* [4–6].

In addition, an important factor for protein production is the formation of disulfide bridges. The reducing properties of *E. coli* cytoplasm prevent disulfide bridges from being formed. Lack of, or defective, disulfide bridges in combination with high expression rates often lead to agglomeration of the target protein resulting in insoluble inclusion bodies (IB), which are biologically inactive and must be resolved in a separate process step [7,8]. To circumvent this problem, the target protein can be expressed as a fusion protein with a signal sequence that controls transport into the periplasmic space. The oxidizing conditions prevailing there allow more efficient formation of disulfide bridges, allowing the target

protein to be obtained in soluble form. In addition, localization in the periplasmic space offers the advantage of fewer host-specific impurities, such as host proteins or DNA, being present there, which means that the target protein can be obtained in higher purity with the aid of a suitable lysis strategy.

Due to various mutations that are beneficial to the process, *E. coli* K12 and B derivatives represent the most commonly used *E. coli* strains [9]. These include reduced acetate formation as well as the absence of host proteases in BL21 strains [10]. In BL21 (DE3), the OmpT and Lon genes are deleted, preventing expression of the corresponding proteases. These proteases are responsible for the degradation of many extracellular and foreign proteins [7]. Deficiency is therefore associated with higher productivity.

Another important factor in productivity is the choice of expression vector. The promoter, selection marker, fusion proteins, and origin of replication play important roles [9,11]. The latter influences the number of plasmid copies in the cell. In this context, a high plasmid copy number does not necessarily equate to high expression; on the other hand, low plasmid copy numbers are also usually disadvantageous in terms of productivity [12]. The use of inducible, strong promoters allows high productivity with simultaneous control over the onset of expression [13,14].

Quality-by-Design (QbD)-based process development is increasingly becoming the standard in the biopharmaceutical industry and is also required by regulatory authorities, such as the FDA and EMA [15,16]. By applying QbD methods, a relationship can be established between the critical process parameters and the relevant quality characteristics of the product. This requires design spaces that can be defined using validated process models [17,18]. This avoids out-of-specification (OOS) batches and ensures that the quality target product profile (QTPP) is met [19,20]. Within design spaces, consistent product quality can be ensured from development through piloting to production [19,21]. In addition to spanning design spaces, validated process models are suitable for real-time prediction of quality attributes, enabling adaptation and optimization of the process due to changing process requirements even after submission [22]. For this purpose, the process models must be developed as “digital twins” (DT). In addition to the digital representation of the process, these enable the realization of advanced process control [23,24].

Such a digital twin can be divided into five levels (see Figure 1), with the level of detail increasing as the level rises. Purely digital models are represented by the first three levels. The first level is a purely stationary, time-independent model. It describes the process by means of simple mass and energy balances and is used for initial optimization and calculation procedures in the first design phase of the process [25–28]. If the steady-state model is extended by accumulation terms and the system dynamics, the second stage of a digital twin is reached. These models are dynamic, time-dependent models, since all variables of interest are derived according to time. They are used for identification of optimal operating conditions, scaling planning, and process control [28–31]. A dynamic model validated with process data, is the third and thus final stage of a purely digital model. A validated model considers phenomena such as inhibitions, which leads to an increase in states. In addition, equipment conditions, such as working power and hydraulics, are taken into account. Models that can be run in real time by receiving automatic inputs through a data link with the physical process are called digital shadows. They represent the fourth stage of a digital twin [32]. With the help of model-based control, the fifth stage of a digital twin, we enable online optimization of the process. In addition, control structures can be applied based on the model-based predictions. Thus, closed-loop process control in real time is enabled by the digitization infrastructure [28].

The workflow of a QbD-based process development is shown in Figure 2 [16,33]. First, the quality target product profile is defined, which influences the bioavailability, potency, and stability of the drug. Thus, the relationship between the QTPP and the quality, safety, and efficacy of the drug can be established [34]. Subsequently, critical quality attributes (CQAs) must be defined and classified, as they are the basis for further process development. By controlling the CQAs within a certain limit, range, or distribution, the desired product

quality can be achieved [35–37]. Consequently, they must be dynamically adjusted as new knowledge is gained about the process or product. Experiments or risk management are used to define the CQAs. The latter includes risk assessment, which should be performed at the beginning of QbD-based process development [35,38]. The definition of the design space in which consistent product quality can be ensured follows the risk analysis and is traditionally done by experimentation. The experimental effort can be reduced by using statistical design-of-experiments (DoE) and rigorous process models [39]. The use of process models becomes feasible when the model used is at least as accurate and precise as the experiments it is designed to replace. This requirement can be verified using Monte Carlo simulation studies by comparing the simulated results with the experimentally obtained data. By using predictive process models, in addition to the resource-efficient spanning of the design space, a quantitatively defined and knowledge-based process optimum can be determined. Consequently, process development becomes not only empirically possible, but is extended by a model- and data-based process evaluation. In addition, physicochemical models do not lose their validity even if the limits of the design space are exceeded [35].

Spanning the design space is followed by the development of a control strategy. This is supported by process analytical technologies (PAT). This PAT-supported control strategy, in combination with digital twins, provides the basis for an automated, continuous process, and also leads to a shortened time-to-market. It also reduces the burden on personnel by reducing both cleaning and sterilization efforts. PAT also enable real-time release testing (RTRT) [35,40]. The development of PAT strategies based on spectroscopic methods has already been demonstrated using various substance systems [40–42]. The final step of the holistic QbD approach involves continuous improvement [35,40]. Thus, a process developed in this way allows better utilization of costly raw materials such as fermentation and feed media. Furthermore, a process developed according to QbD guidelines can reduce logistical expenses [23,42–45].

This article presents the application of digital twins in the context of a QbD concept. Figure 3 gives an overview of the process.

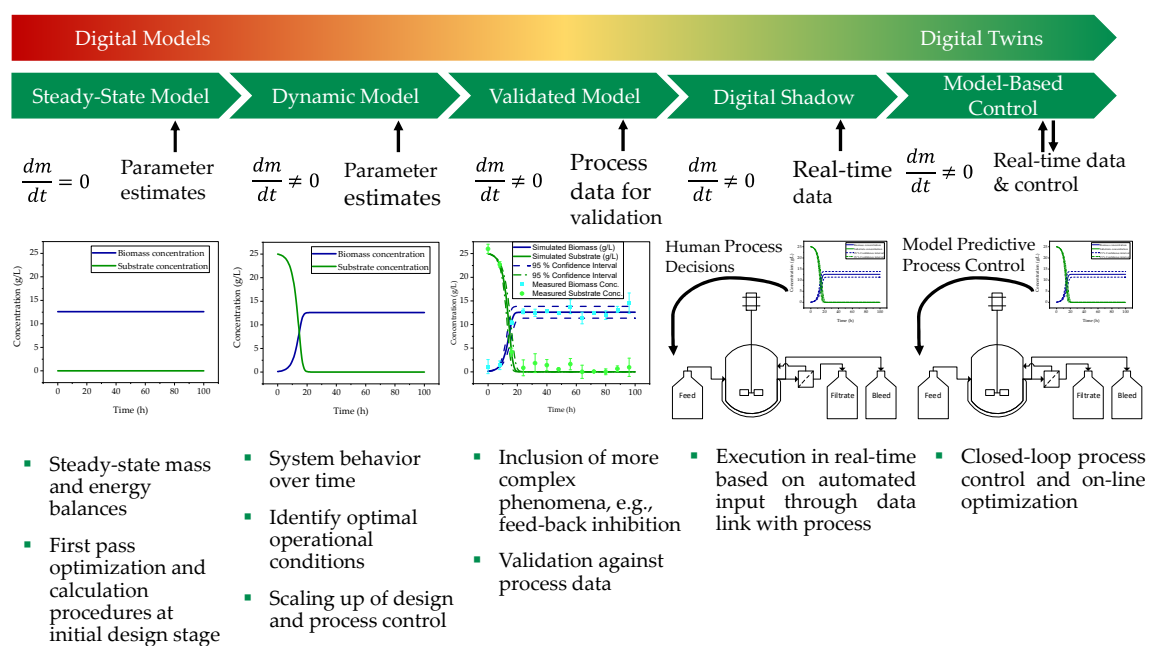


Figure 1. Levels of a digital twin, starting from a steady-state model, over a dynamic model, a validated model, and a digital shadow to a model-based control.

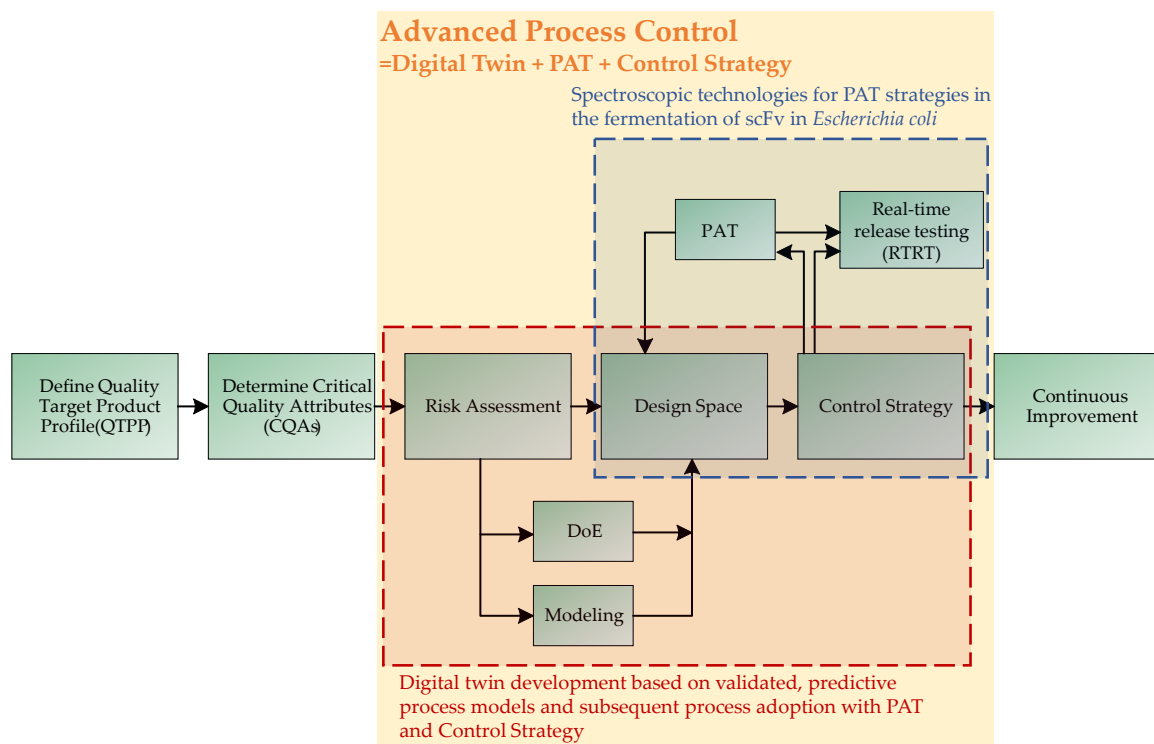


Figure 2. Workflow of model validation based on a QbD-oriented approach. In the first step, the QTPPs are defined. Subsequently, the CQAs are defined and a risk assessment of the influence of various process parameters on the CQAs is carried out. The risk assessment results in a design space for the process parameters to be investigated, which can be examined either via experiments or by means of a rigorous process model. Based on the results, a control strategy is defined, which can be continuously compared online via PAT with the actual state of the system. Strict implementation of this strategy allows continuous process optimization.

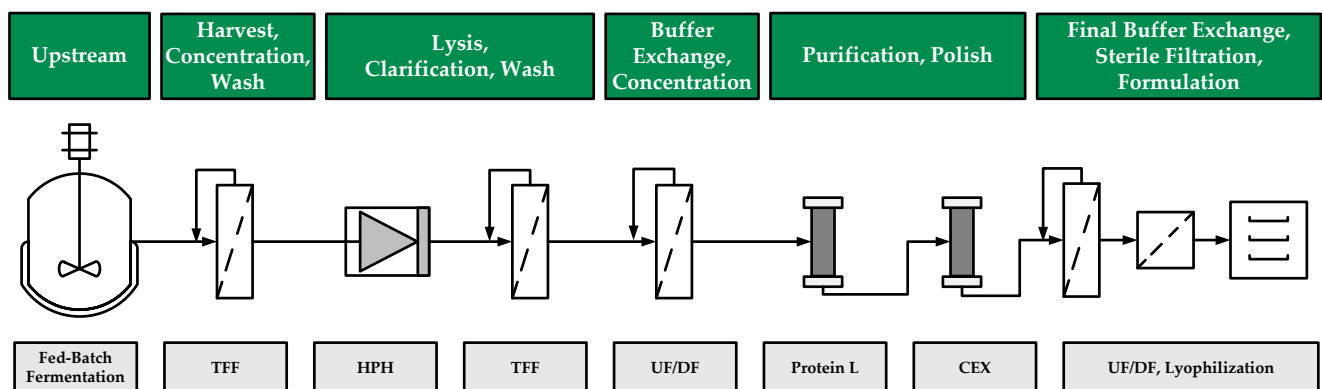


Figure 3. Process overview of the production of scFv. The process starts with fermentation of *E. coli*. Cells are harvested and washed by TFF, and subsequently lysed through HPH to release the intracellular product. The scFv is leached by TFF, concentrated and buffer exchanged by UF/DF and finally purified and polished through Protein L and CEX chromatography, respectively. Fill-and-finish is done by buffer exchange and lyophilization.

2. Materials and Methods

2.1. Fed-Batch Fermentation

Fed-Batch cultivations were described using a Monod-based model where glucose was included as the carbon source. The concentration of viable cells, X_V , was described by

$$\frac{dX_V}{dt} = \frac{(\dot{V}_{in} \cdot X_{V,in} - \dot{V}_{out} \cdot X_{V,out})}{V} + \mu \cdot X_V \cdot \left(1 - \frac{X_V}{X_{V,max}}\right)^m \quad (1)$$

where μ is the growth rate that was described by a Monod equation

$$\mu = \mu_{max} \cdot \frac{[GLC]}{K_{glc} + [GLC]} \cdot \frac{[O_2]}{K_{O_2} + [O_2]} \quad (2)$$

The glucose concentration was described by the following equation in which m_{glc} is the maintenance coefficient of glucose

$$\frac{d[GLC]}{dt} = \frac{(\dot{V}_{in} \cdot [GLC]_{in} - \dot{V}_{out} \cdot [GLC]_{out})}{V} - \left(\frac{\mu}{Y_{X_V/gluc}}\right) \cdot X_V \quad (3)$$

The yield coefficient of biomass from glucose, $Y_{X_V/gluc}$, is composed of a growth-independent, $Y_{X_V/Glc,growth}$, and a growth-dependent term, $q_{Glc/Xm}$

$$Y_{X_V/gluc} = Y_{X_V/Glc,growth} + q_{Glc/Xm} \cdot \frac{1}{\mu} \quad (4)$$

The change in the oxygen concentration was calculated based on the oxygen transfer and the oxygen consumption by the viable biomass

$$\frac{dc_{O_2}}{dt} = k_L a \cdot (c_{O_2}^* - c_{O_2}) - q_{O_2} \cdot X_V \quad (5)$$

where $k_L a$ is the specific oxygen transfer coefficient, $c_{O_2}^*$ is the oxygen saturation concentration in the fermentation broth, c_{O_2} is the current oxygen concentration in the fermentation broth and q_{O_2} is the specific oxygen uptake rate.

The specific product formation was proportional to the viable cell concentration

$$\frac{d[scFv]}{dt} = \frac{(\dot{V}_{in} \cdot [scFv]_{in} - \dot{V}_{out} \cdot [scFv]_{out})}{V} + q_{scFv} \cdot X_V \quad (6)$$

\dot{V} is the volumetric flowrate either in or out of the reactor, and V is the cultivation volume. The change in volume over time was calculated using a volume balance:

$$\frac{dV}{dt} = \dot{V}_{in} - \dot{V}_{out} \quad (7)$$

Since the process considered in this study is a fed-batch cultivation, the outflowing volume flow is zero.

2.2. Ultrafiltration/Diafiltration

The investigated hollow fiber module consists of 60 fibers (0.5 mm inner diameter, 0.2 m length, 115 cm² surface area, 500 kDa MWCO). The process model applied is based on work by Grote et al. [46]. Filtration is described by the Darcy–Weisbach equation [47–49]

$$J_v = \frac{TMP}{\eta \times R} \quad (8)$$

The three major approaches to model flux decline in tangential-flow ultrafiltration are resistance, gel-concentration, and osmotic-pressure models [50]. Since the retentate stream is a suspension of *E. coli* cells and bioparticles, flux decline is best described by the resistance model, where the total resistance R is the sum of the initial membrane resistance R_m and the boundary-layer resistance R_{bl} , which is computed from experiments [51,52]. The transmembrane pressure TMP is defined by Equation (9):

$$\text{TMP} = \frac{P_{ret,in} - P_{ret,out}}{2} - P_{per} \quad (9)$$

For process simulations all model parameters are randomly varied inside the experimentally observed range to show model prediction precision and accuracy. Based on 31 simulations the experimental results are then compared to the simulation range of prediction.

2.3. Chromatography

There are different approaches for the purification of single-chain fragment variables (scFv). Most commonly, scFv are purified employing a metal-ion affinity chromatography to capture scFv from the stock through His-tag modification [53]. Alternatively, to the metal-ion affinity, chromatography Protein L chromatography has gained track in recent years [54]. In addition, cation-exchange chromatography or different mixed-mode chromatography techniques can be used in the purification of these fragments [55]. In comparison with metal affinity chromatography, these techniques do not need a Histidine-tagged protein, which most likely would have to be cleaved before its usage in a pharmaceutical application, which is why we decided to use Protein L chromatography as the purification and cation exchange chromatography as the polishing step.

For protein L chromatography we used the Toyopearl® AF-rProtein L-650 F skillpak 1 mL column (Tosoh Bioscience GmbH, Griesheim, Germany). For cation exchange chromatography we used the BioPro IEX SmartSep S30 1 mL column (YMC Europe GmbH, Dinslaken, Germany). We based our method design for Protein L on literature data [54] and employed a five-column volume (CV) gradient from buffer A to buffer B. Buffer A consisted of 50 mM sodium citrate (pH 6.5) and buffer B consisted of 50 mM sodium citrate (pH 2.3); subsequently, to the load, we washed the column for 10 CV and used a 10 CV regeneration with 0.1 M NaOH. For cation exchange chromatography, we used a 5 CV gradient in conjunction with a 3 CV wash step and a 3 CV regeneration, based on a prior method screening. In the cation exchange chromatography, buffer A consisted of 50 mM sodium phosphate (pH 3.5), and buffer B consisted of 50 mM sodium phosphate, and 1 M sodium chloride (pH 5.5).

The Digital Twin for chromatography can either use a general rate model or a lumped pore diffusion model [56–58]. In this case study, a lumped pore diffusion model of chromatography was used; as for scFv, it can be expected that pore diffusion does not show a major impact on the chromatogram. This is supported by the relatively low impact on monoclonal antibodies, which are considerably larger [58,59]. The mass balance of the stationary phase for the lumped pore diffusion model is [56]:

$$\varepsilon_{p,i} \cdot \frac{\partial c_{p,i}}{\partial t} + (1 - \varepsilon_{p,i}) * \frac{\partial q_i}{\partial t} = \frac{6}{d_p} \cdot \frac{(1 - \varepsilon_S)}{\varepsilon_S} \cdot k_{eff,i} \cdot (c_i - c_{p,i}) \quad (10)$$

With $\varepsilon_{p,i}$ as the porosity of the component, $c_{p,i}$ as the concentration of the component in the pores, t as the time, q_i as the loading, d_p as the mean diameter of the resin particle, ε_S as the voidage, $k_{eff,i}$ as the effective mass transport coefficient, and c_i as the concentration in the continuous phase.

Different approaches for modelling of adsorption have been described by different working groups [56,59–62]. In this study, adsorption is modelled using a Langmuir isotherm [61,63]

$$q_i = \frac{q_{max,i} \cdot K_{eq,i} \cdot c_i}{1 + K_{eq,i} \cdot c_i} \quad (11)$$

Here, $q_{max,i}$ is the maximum loading capacity of the component and $K_{eq,i}$ is the Langmuir coefficient of the component. $K_{eq,i}$ and $q_{max,i}$ are related by the Henry coefficient H_i , see Equation (12) [56]. Salt influence can be described by Equations (13) and (14) defining a_1 , a_2 , b_1 , and b_2 as material constants [59,64].

$$q_{max,i} \cdot K_{eq,i} = H_i \quad (12)$$

$$q_{max,i} = b_1 \cdot c_{p,1} + b_2 \quad (13)$$

$$H_i = a_1 \cdot c_{p,1}^{a_2} \quad (14)$$

The mass transfer coefficient $k_{eff,i}$ is given by Equation (15). Here, $k_{f,i}$ is the film mass transfer coefficient, r_p the particle radius, and $D_{p,i}$ the pore diffusion coefficient.

$$k_{eff,i} = \frac{1}{\frac{1}{k_{f,i}} + \frac{r_p}{D_{p,i}}} \quad (15)$$

$D_{p,i}$ is calculated according to the correlation of Carta [65] and $k_{f,i}$ according to Wilson and Geanoplis [66].

2.4. Lyophilization

As the last step in the production of the scFv solution lyophilization is used to formulate the product into a stable solid form. A one-dimensional sorption sublimation model introduced by Klepzig et al. models the Lyophilization process [67]. Here, the exact derivation of the proposed model is shown. It calculates the time-dependent product temperature and the residual moisture during the lyophilization process with a coupled mass and heat transfer. The process is separated into primary and secondary drying. In both drying steps, conduction is the main heat transport mechanism.

The energy balance is written as:

$$\rho_{Product} \cdot c_{p,apparent} \cdot \frac{\partial T}{\partial t} = \lambda \cdot \frac{\partial^2 T}{\partial x^2} \quad (16)$$

$\rho_{Product}$ describes the density of the product, $c_{p,apparent}$ is the apparent heat capacity, T the product temperature inside the vial, and λ is the heat conductivity.

In primary drying, the ice is removed by sublimation and convection through the dried zone. The phase change at the sublimation interface is implemented by the apparent heat capacity.

The overall mass balance of water considers ice and the dried product. Convection controls the transport rate.

$$\frac{\partial m_W}{\partial t} = \left(\rho_{W,g} \cdot \frac{\Delta p}{\eta_W \cdot K} \cdot A_{vial} \right) \quad (17)$$

With m_w as overall water mass, $\rho_{W,g}$ as density of water vapor, Δp as pressure difference, η_W as dynamic vapor viscosity of water, and K as hydraulic flow resistance, A_{vial} as cross-sectional area of the vial. Heat and mass transfer are coupled by the sublimation enthalpy [68].

In secondary drying, bound water from the dried matrix is removed by desorption. It is modeled by an Arrhenius approach. The mass balance of the bound water can be formulated to:

$$\frac{\partial w_{bw}}{\partial t} = - \exp\left(-\frac{\Delta h_{subl}}{R \cdot T_{product}}\right)^{a_w} \cdot (w_{bw} - w_{bw,eq}) \quad (18)$$

With w_{bw} as mass fraction of the bound water in the dried product, Δh_{subl} as sublimation enthalpy, R as gas constant, a_w as water activity, and $w_{bw,eq}$ as mass share of bound water at equilibrium.

3. Results

3.1. Fed-Batch Fermentation

Fed-batch fermentation of *E. coli* BL21(DE3) transformed with pET22b(+) carrying the scFv gene under the control of the T7-promoter, was performed for 19 h. Riesenberg's medium with an initial glucose concentration of 8.8 g/L as well as 10 g/L yeast extract and 5 g/L soy peptone was inoculated with an initial dry cell weight of 0.5 g/L. The fermentation was done at 37 °C, pH 6.9 and 2000 rpm stirrer speed, using a Rushton turbine with 54 mm diameter. Gassing was constant at 2 vvm using air and pure oxygen so to keep the pO₂ above 20 %. The batch phase lasted 5 h after which the exponential glucose feeding was started to reach a constant growth rate of 0.15 h⁻¹. After four more hours the feeding profile was adjusted to reach a constant growth rate of 0.05 h⁻¹. The expression of the scFv encoding gene was induced by addition of 1 mM IPTG after 12 h. Figure 4 shows the experimental and simulation results of 30 Monte-Carlo simulations of the fed-batch fermentation. The model can predict the growth of the cells and the consumption of glucose sufficiently. Only at the end of the fermentation, the biomass is slightly underestimated. The final scFv concentration after HPH was 0.74 ± 0.02 g/L, which is equivalent to 13.7 ± 0.4 mg/g.

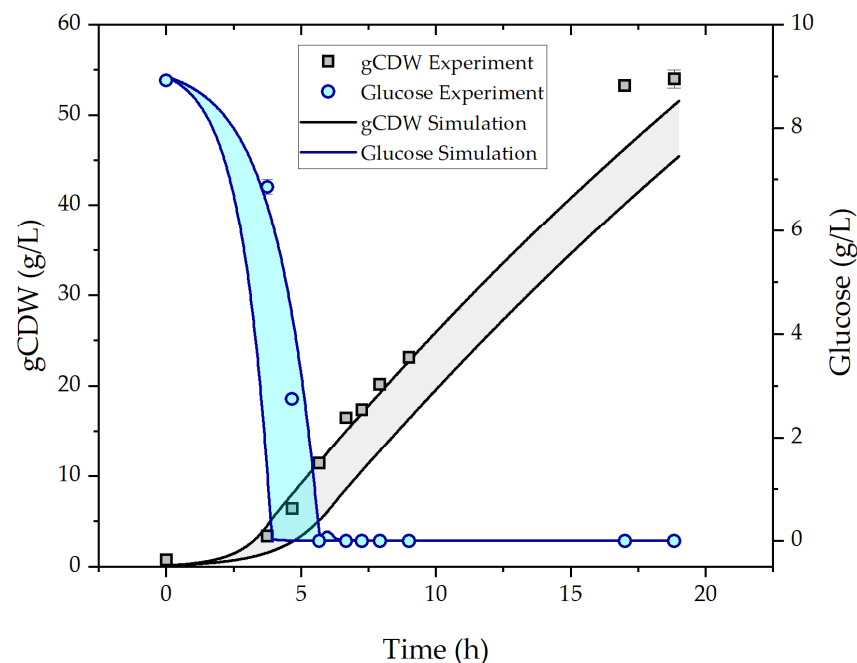


Figure 4. Experimental and simulation results of dry cell weight and glucose concentration of the *E. coli* fed-batch fermentation.

3.2. Harvest by UFDF

After fermentation, cell harvest was performed by ultra/diafiltration. This process step can be divided into two steps: volume reduction and concentration by a factor of three

and subsequent washing with five diafiltration volumes (DV). Concentration reduces the amount of buffer required in the following diafiltration step. The process model prediction of three experiments differing in applied transmembrane pressure (TMP), shear rate, and cell concentration used is shown in Figure 5. The prediction of the digital twin is in line with the experimental data. Both the strong decrease in the flux (J_v) at the beginning and the slower decrease in the flux in the further experimental process due to the increase in the boundary layer resistance are reproduced.

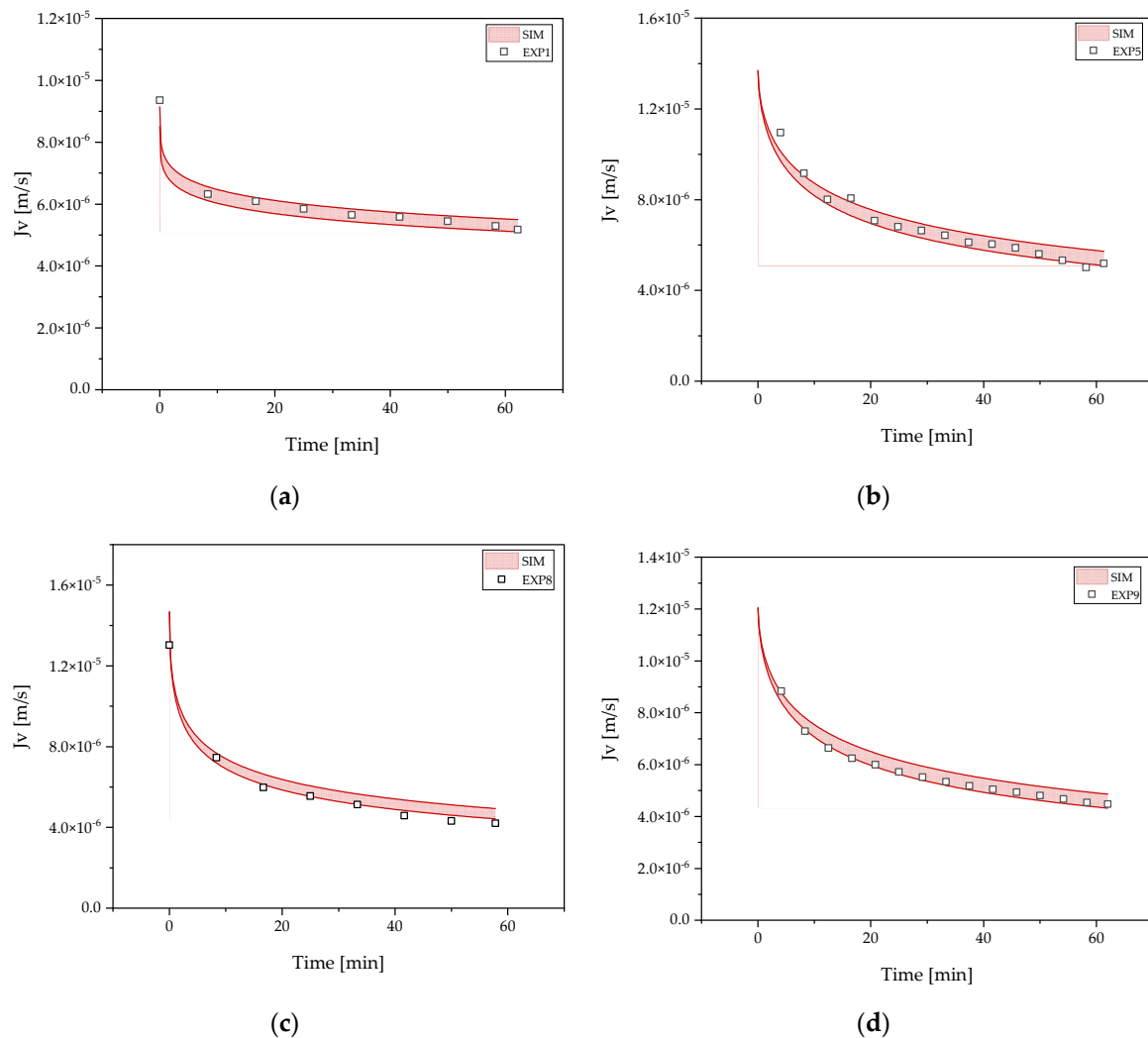


Figure 5. Flux J_v over time for experimental (squares) as well as digital twin prediction (red area) for harvest experiments by ultra-/diafiltration: (a) Experiment 1 (EXP1): 1.3 bar transmembrane pressure (TMP), 2040 s^{-1} shear rate. (b) Experiment 5 (EXP5): 1.4 bar TMP, $11,285 \text{ s}^{-1}$ shear rate. (c): Experiment 8 (EXP8): 1.3 bar TMP, 6072 s^{-1} shear rate. (d): Experiment 9 (EXP9): 0.8 bar TMP, 6028 s^{-1} shear rate.

In order to demonstrate the predictive power of the digital twin, the time from which the filtration course can be predicted and the end point determined was investigated. Figure 6 shows that the blocking mechanism including the blocking constant can already be identified after one third of the total process time. Thus, the digital twin, which is continuously fed with the process data in real time, can predict the further course of the process at an early stage, compare it with predefined limits and, if necessary, carry out an optimization.

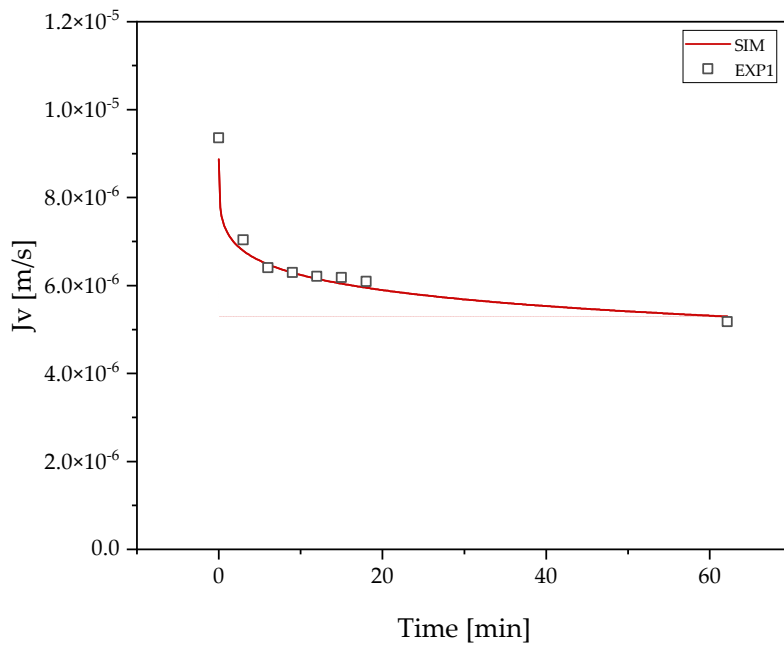
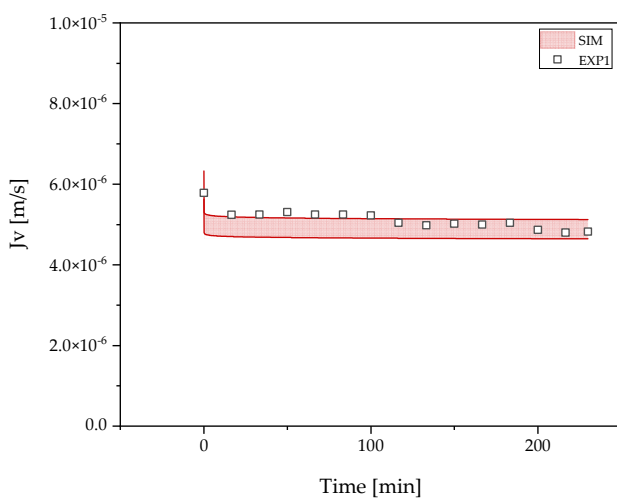


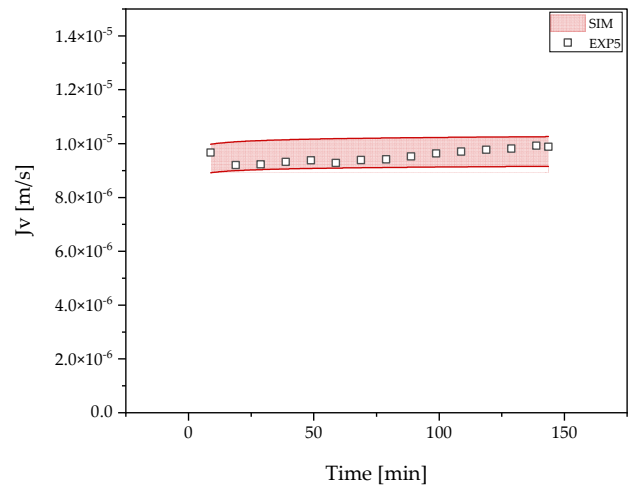
Figure 6. Demonstration of early digital twin-assisted prediction of the filtration progress as well as endpoint determination.

3.3. Clarification by UFDF

After cell lysis, the homogenizate is clarified by ultra-/diafiltration. The target component is leached out over five diafiltration volumes. The process model prediction of three experiments differing in applied transmembrane pressure (TMP), shear rate, and applied concentration is shown in Figure 7. The concentration used is corresponding to the concentration factor in ultra-/diafiltration used for cell harvest. The prediction of the digital twin agrees with the experimental data. The strong decrease in flux (J_v) is predicted, as well as the subsequent flux, which is approximately constant.



(a)



(b)

Figure 7. Cont.

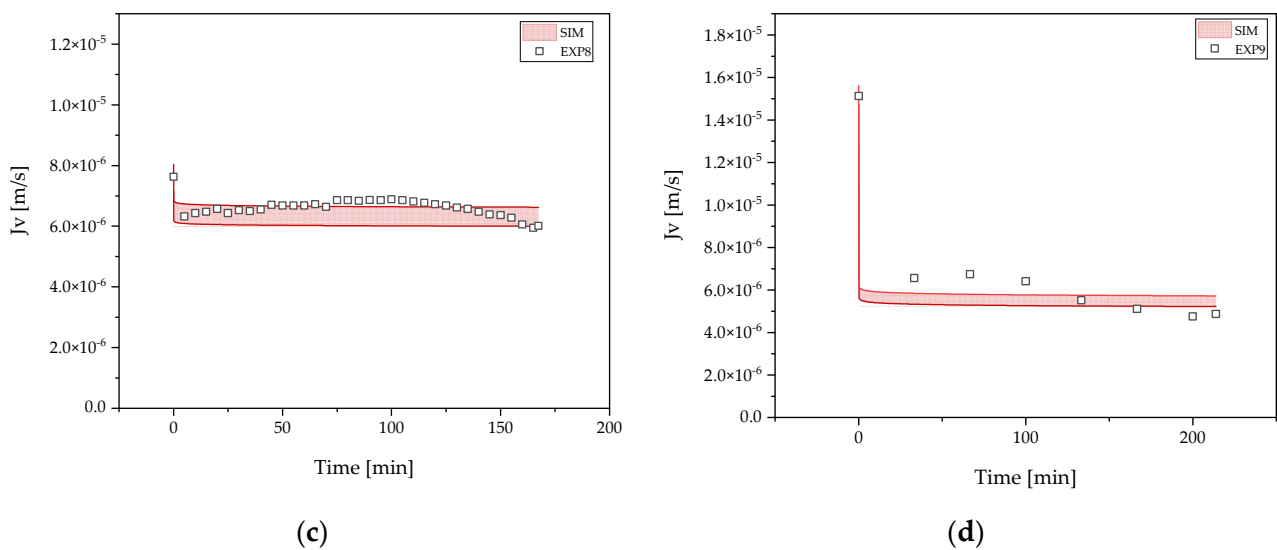


Figure 7. Flux J_v over time for experimental (squares) as well as digital twin prediction (red area) for clarification experiments by ultra-/diafiltration: (a) Experiment 1 (EXP1): 1.4 bar transmembrane pressure (TMP), 2062 s^{-1} shear rate. (b) Experiment 5 (EXP5): 1.3 bar TMP, $11,633 \text{ s}^{-1}$ shear rate. (c): Experiment 8 (EXP8): 1.3 bar TMP, 6071 s^{-1} shear rate. (d): Experiment 9 (EXP9): 0.8 bar TMP, 6085 s^{-1} shear rate.

3.4. Concentration and Buffer Exchange by UFDF

After clarification of the homogenized suspension volume reduction and buffer exchange is done by ultrafiltration/diafiltration. This process step can be divided into two phases. First, a concentration step is performed to reduce the subsequently needed exchange buffer volume as well as process time. Second, buffer exchange and partial purification is achieved by diafiltration with five diafiltration volumes (DV). Process model prediction are shown in Figure 8. The digital twin prediction for experiments aligns with the experimental results regarding ultrafiltration endpoint.

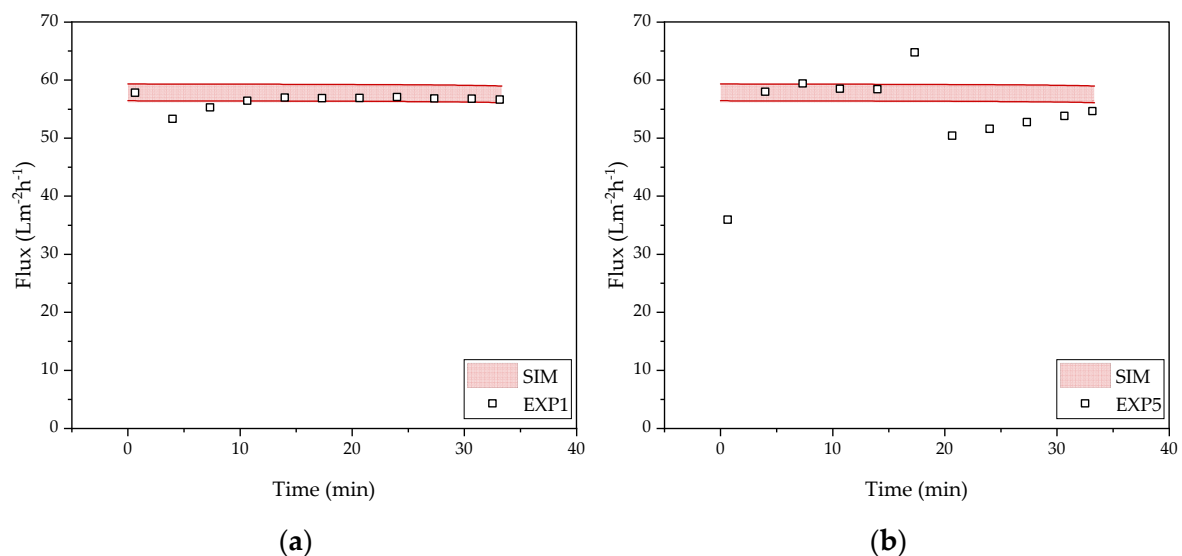


Figure 8. Cont.

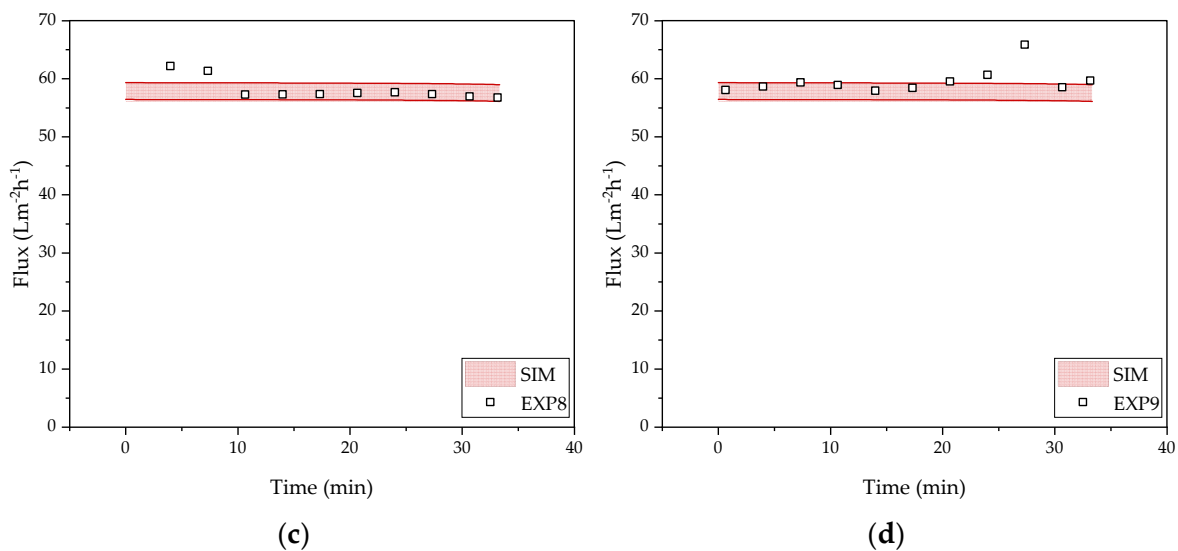


Figure 8. Flux J_v over time for experimental (squares) as well as digital twin prediction (red area) for buffer exchange experiments by ultra-/diafiltration after clarification with experimental conditions: (a) Experiment 1 (EXP1): 1.4 bar transmembrane pressure (TMP), 2062 s^{-1} shear rate. (b) Experiment 5 (EXP5): 1.3 bar TMP, $11,633 \text{ s}^{-1}$ shear rate. (c): Experiment 8 (EXP8): 1.3 bar TMP, 6071 s^{-1} shear rate. (d): Experiment 9 (EXP9): 0.8 bar TMP, 6085 s^{-1} shear rate.

3.5. Purification by Protein L Chromatography

For the Protein L Digital Twin, we based our calculations on the data given by the resin supplier, especially for the resin particle size, pore size, and operating velocity ranges. Isotherm parameters were determined using a least-squares routine in combination with the experimentally obtained data. The results are shown in Figure 9. For the scale-up of the purification step, we used the determined parameters and increased velocity according to the resin supplier's information sheet to 500 cm/h; additionally, we decreased the wash volume in the chromatographic method to 3 CV. This results in a productivity of $5.31 \text{ g/L}\cdot\text{d}$, with a high process yield in the obtained fraction of 96%.

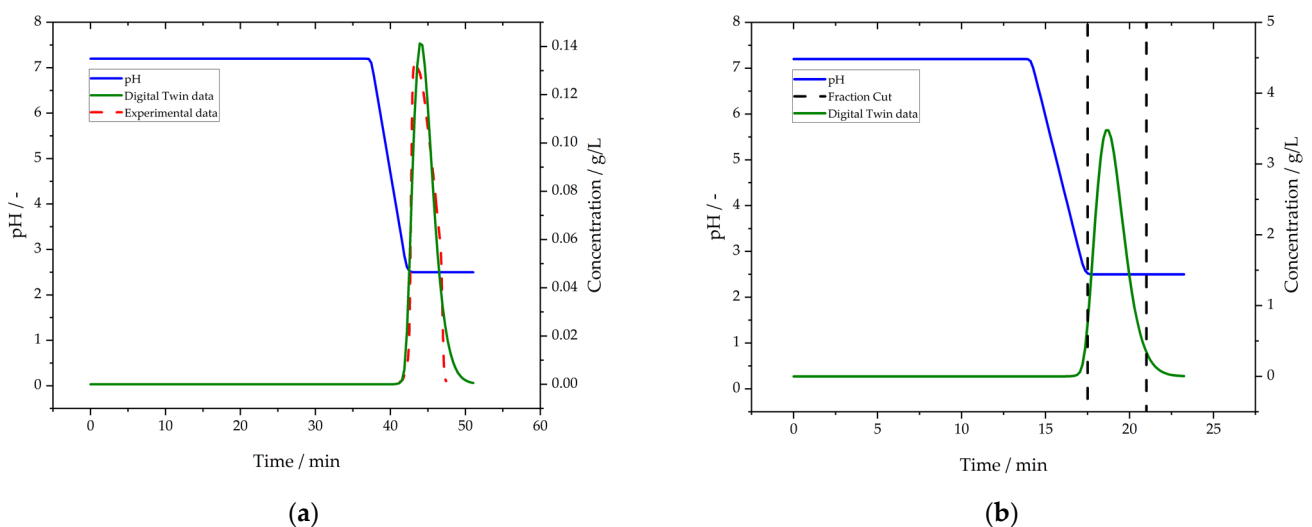


Figure 9. Chromatograms for the laboratory process (a) and the scaled-up process (b). The dashed red line gives the experimental data, black shows a theoretical fraction cut, the solid green lines give the data derived from the Digital Twin and the solid blue lines give the gradients.

3.6. Polishing by Cation Exchange Chromatography (CEX)

In CEX chromatography, the side components are mostly non-binding components, obtained during the wash from one to three minutes, see Figure 10. As such, a very pure product is obtained, with no identifiable side components in the analytics. The product is obtained in one CV, which would allow for a good concentration factor in this step. For the evaluation of a potential scale-up, however, we have to rely on literature data for the maximum loading capacity of the resin, as a production of scFv on a preparative scale to evaluate the CEX chromatography thoroughly was unfeasible in the context of this study. We decided to assume the capacity given by the supplier.

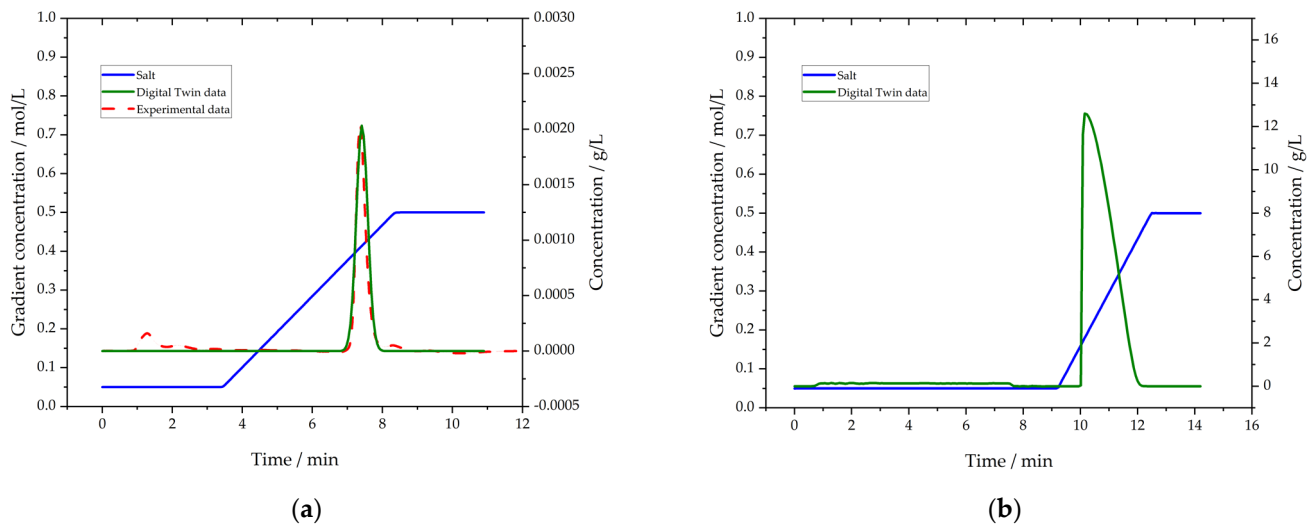


Figure 10. Chromatogram of the laboratory ion exchange chromatography (a) (dashed) and scaled-up process (b) with the digital twin results (green solid), respectively. The gradient is given as a blue solid line.

As before, we used the product of the Protein L chromatography as the feed for the following unit operation. The feed volume was 42 mL, which was scaled up to a velocity of 500 cm/h. This scale up results in a 2167 g/L·d, the yield was 96%, and the concentration factor was 3.9, ending up with a product concentration after CEX chromatography 8 g/L.

3.7. Formulation by Lyophilization

In this study, 266 2R vials were filled with 500 μ L scFv solution and then freeze-dried. This scale is manageable with an Epsilon 2-4 LSC-plus [69]. The main excipient was mannitol. The vial heat transfer coefficient was taken from the literature [67]. Since the main excipient was mannitol, the hydraulic flow resistance from this study is increased. The so-called edge effect leads to a drying batch heterogeneity because edge vials receive a higher amount of energy [70]. Edge vials receive the highest heat input, whereas center vials are limited to conduction. The lyophilization process for different vials is shown in Figure 11.

The drying protocol was adopted from literature [71]. Figure 11 shows the results from the digital twin of the freeze drying process. During primary drying the shelf temperature was raised from -40 $^{\circ}$ C to -23 $^{\circ}$ C and a chamber pressure of 0.18 mbar was set. The primary drying step lasted approximately 16 h. During secondary drying the shelf temperature was increased to 15 $^{\circ}$ C and the pressure was lowered to 0.001 mbar. During primary drying, the product temperature was gradually increased to the shelf temperature. Edge vials finished primary drying faster. Furthermore, the edge effect resulted in an increased product temperature compared to the center vial. Both vial classes finished primary drying before secondary drying had started. The endpoint of the primary drying can be determined as the point where the product and shelf temperature were the same. In

secondary drying, the residual moisture was set. The final residual moisture of the vials was about <1%.

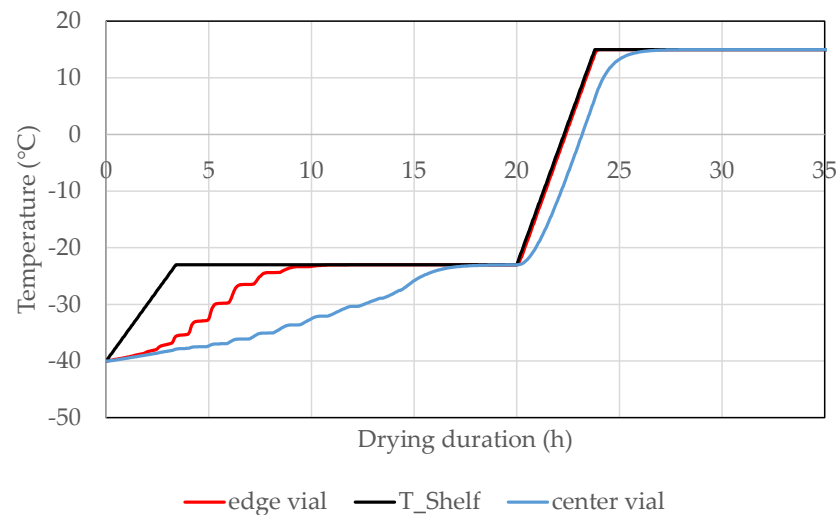


Figure 11. Shelf and product temperature profiles.

4. Discussion

In pharmaceutical process development, the QbD concept is increasingly important. During the process run, it must be constantly ensured that the process is operated within PAR. Spectroscopic methods such as Raman and FTIR spectroscopy allow real-time process control with respect to critical process parameters. This information can be passed on to the digital twins of the process, allowing early prediction of process performance and, thus, ensuring robust process control. In this study, using the production of scFv in *E. coli* as an example, it was shown that the entire process, starting with fermentation, and subsequently through several purification steps to formulation, can be well predicted across all basic operations using the process models employed.

In fermentation, the progression of biomass, glucose, as well as product concentration can be accurately and precisely predicted. The model can be used to control glucose feeding, pH as well as pO₂ control. The biomass and product concentration prediction can also be fed to the subsequent process models to adjust the operating parameters accordingly.

After fermentation, the fermentation broth is first concentrated via tangential flow filtration and then washed with PBS (UF/DF). The digital twin can accurately predict the flux across the membrane as a function of TMP and shear rate. Thus, in the process, the model can predict biomass and product concentration on the one hand, and depending on the operating parameters, predict filtration time based on increasing blockage due to increasing top layer resistance. Depending on the blockage, the TMP, as well as the shear rate, can be adjusted based on the model prediction and thus be operated as gently as possible. Fluctuating biomass concentrations from the fermentation can also be taken into account in real time and the operating parameters adjusted accordingly to achieve consistent concentration and defined washing.

The washing step is followed by mechanical cell disruption using a high-pressure homogenizer. After disruption, the scFv is clarified by tangential flow filtration. Analogous to the harvest, the digital twin can be used to predict, monitor, and control the washing. The model is able to predict the experimentally determined permeate fluxes predictively. In addition, in combination with PAT, for example, FTIR, the digital twin allows dynamic adjustment of the exchange volumes used based on the current desalination level and purity. This flexibility cannot be achieved with conventional process development and offline analytics, where exchange volumes are fixed. Consequently, only a digital twin and QbD-based process development can achieve optimal product purity or save buffers.

The clarification step is followed by protein L chromatography in which the scFv is bound from the mobile phase by affinity. The digital twin in the chromatography was able to predict well the experimentally determined process course based on the manufacturer’s data on the adsorbent used, as well as the experimentally determined parameters for the isotherms. Using the model, the flow rate could be increased, and the wash step reduced to 3 DV, allowing the process to be run more efficiently. As a result, a productivity of 5.3 g/L/d at a purity of 96% can be achieved. Furthermore, the process model is able to accurately predict elution time points, which can control fractionation of the product.

Protein L chromatography is followed by polishing using CEX chromatography. Analogous to protein L chromatography, the process model can be used to increase efficiency in terms of throughput. As a result, a productivity of 2167 g/L/d at a yield of 96% is achieved. The product concentration after CEX is 8 g/L.

After polishing, freeze drying is performed to ensure long-term stability. The digital twin in freeze drying can be used to enable efficient process control in terms of drying time while avoiding collapse of the cake. The primary variables influencing drying are shelf temperature, temperature gradient, chamber pressure, and residual moisture in the dried product. These can be controlled or predicted by the digital twin. Furthermore, the model allows a prediction of the heterogeneity of the vials depending on the position in the freeze dryer (corner vs. center).

The use of digital twins makes it possible to realize more efficient process management in several respects, as shown in Figure 12. On the one hand, it is possible to predict the exact end points of the process steps at an early stage, so that the preparation of the subsequent basic operations can be optimally prepared and scheduled (Figure 13). Furthermore, PAT in combination with a predefined normal operating range eliminates the need for time-consuming quality controls. All in all, the maximum savings potential is a reduction in the total time for downstream processing by a factor of two, since the downstream can be performed within one working day instead of two.

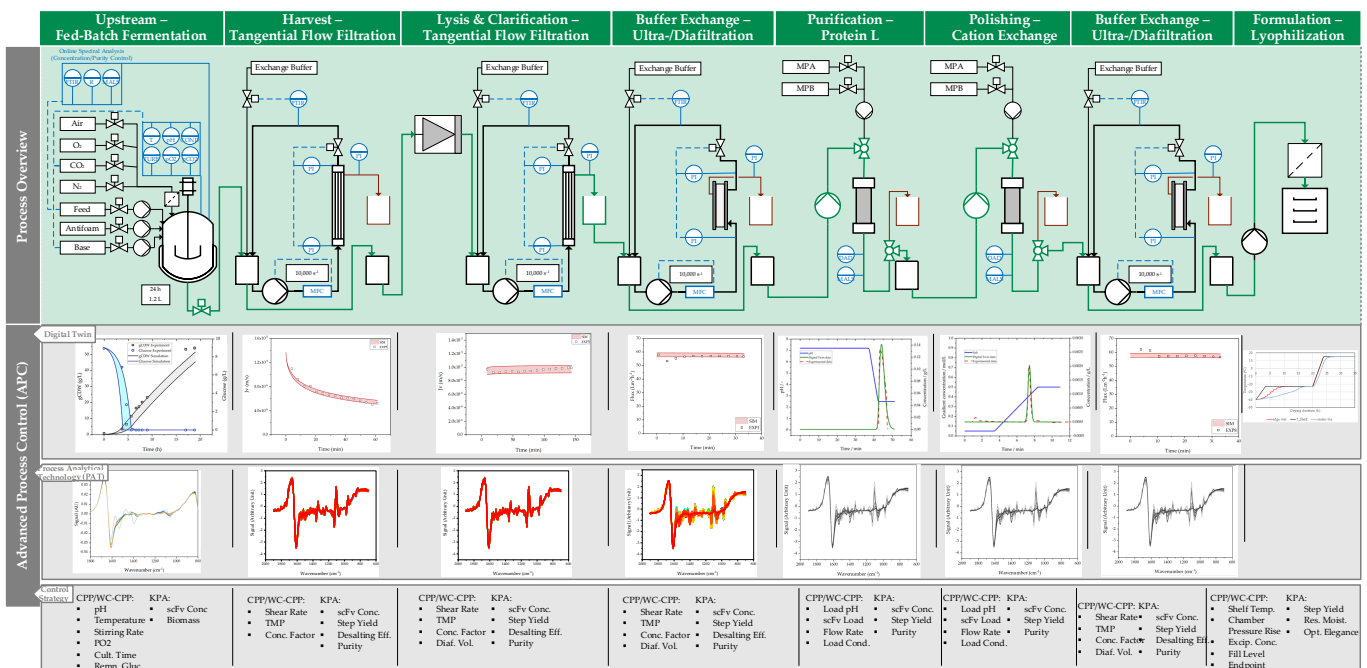


Figure 12. Process flowsheet including APC by Digital Twins and optimized PAT. Critical Process Parameter (CPP), Well-Controlled Critical Process Parameter (WC-CPP), Key Process Attribute (KPA), Particle Size Distribution (PSD), Viable Cell Density (VCD), Transmembrane Pressure (TMP).

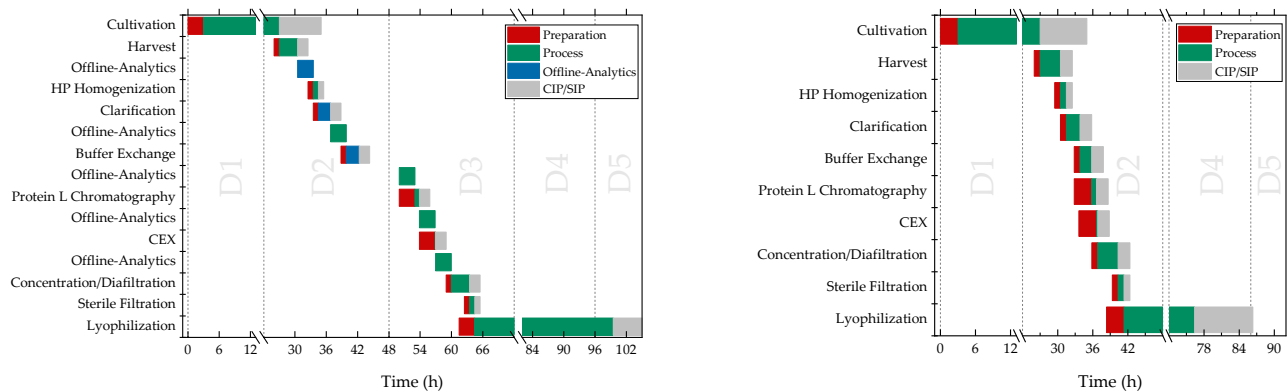


Figure 13. (a) Conventional process schedule based on offline analytics vs. (b) optimized process schedule enabled by PAT for APC and DT.

5. Conclusions

This work demonstrates the application of digital twins for advanced process control using the example of the production and purification of scFv in *E. coli* for a whole process, starting with fermentation and ending with the formulation by freeze drying. The digital twin can predict the concentrations during fermentation, such as glucose, but can also be used for optimization. Knowledge of the ideal harvest time and the resulting product concentration present can be used for optimal preparation of the harvest and concentration via tangential flow filtration, where concentration is increased by a factor of three, and five diafiltration volumes are used for washing. Tangential flow filtration is also applied for clarification after high-pressure homogenization, where the digital twin accurately predicts flux decrease at different operating points within a DoE plan, which enabled shear rate and biomass concentrations to be identified as critical process parameters. In the following Protein L purification and cation exchange chromatography polishing step, the digital twins allow for improvement in terms of duration and productivity. In the final lyophilization step, the digital twin is able to determine the critical residual moisture and endpoint of the drying, depending on the position of the vial in the freeze dryer.

Author Contributions: Conceptualization, J.S.; software, process and analytics experiments, H.H., A.H., A.S., F.L.V. and A.J.; writing—original draft preparation, H.H., A.H., A.S., F.L.V. and A.J.; writing—review and editing, H.H., A.H., A.S., F.L.V., A.J. and J.S.; supervision, J.S.; project administration, J.S. All authors have read and agreed to the published version of the manuscript.

Funding: This research received no external funding.

Data Availability Statement: Data generated in this study are available from the authors upon reasonable request.

Acknowledgments: The authors would like to acknowledge the fruitful discussion with their Clausthal University of Technology colleagues. The authors would like to thank Annika Leibold and Armin Busch for excellent laboratory work and discussion. The authors acknowledge financial support by Open Access Publishing Fund of Clausthal University of Technology.

Conflicts of Interest: The authors declare no conflict of interest.

References

1. Casali, N. *Escherichia coli* host strains. *Methods Mol. Biol.* **2003**, *235*, 27–48. [[CrossRef](#)] [[PubMed](#)]
2. Sørensen, H.P.; Mortensen, K.K. Advanced genetic strategies for recombinant protein expression in *Escherichia coli*. *J. Biotechnol.* **2005**, *115*, 113–128. [[CrossRef](#)] [[PubMed](#)]
3. Terpe, K. Overview of bacterial expression systems for heterologous protein production: From molecular and biochemical fundamentals to commercial systems. *Appl. Microbiol. Biotechnol.* **2006**, *72*, 211–222. [[CrossRef](#)] [[PubMed](#)]
4. Sanchez-Garcia, L.; Martín, L.; Mangués, R.; Ferrer-Miralles, N.; Vázquez, E.; Villaverde, A. Recombinant pharmaceuticals from microbial cells: A 2015 update. *Microb. Cell Fact.* **2016**, *15*, 33. [[CrossRef](#)]

5. Walsh, G. Biopharmaceutical benchmarks 2014. *Nat. Biotechnol.* **2014**, *32*, 992–1000. [[CrossRef](#)]
6. Baeshen, N.A.; Baeshen, M.N.; Sheikh, A.; Bora, R.S.; Ahmed, M.M.M.; Ramadan, H.A.I.; Saini, K.S.; Redwan, E.M. Cell factories for insulin production. *Microb. Cell Fact.* **2014**, *13*, 141. [[CrossRef](#)]
7. Ferrer-Miralles, N.; Domingo-Espín, J.; Corchero, J.L.; Vázquez, E.; Villaverde, A. Microbial factories for recombinant pharmaceuticals. *Microb. Cell Fact.* **2009**, *8*, 17. [[CrossRef](#)]
8. Swartz, J.R. Advances in Escherichia coli production of therapeutic proteins. *Curr. Opin. Biotechnol.* **2001**, *12*, 195–201. [[CrossRef](#)]
9. Tripathi, N.K. Production and Purification of Recombinant Proteins from Escherichia coli. *ChemBioEng Rev.* **2016**, *3*, 116–133. [[CrossRef](#)]
10. Daegelen, P.; Studier, F.W.; Lenski, R.E.; Cure, S.; Kim, J.F. Tracing ancestors and relatives of *Escherichia coli* B, and the derivation of B strains REL606 and BL21(DE3). *J. Mol. Biol.* **2009**, *394*, 634–643. [[CrossRef](#)]
11. Rosano, G.L.; Ceccarelli, E.A. Recombinant protein expression in *Escherichia coli*: Advances and challenges. *Front. Microbiol.* **2014**, *5*, 172. [[CrossRef](#)] [[PubMed](#)]
12. Baneyx, F. Recombinant protein expression in *Escherichia coli*. *Curr. Opin. Biotechnol.* **1999**, *10*, 411–421. [[CrossRef](#)]
13. Studier, F.; Moffatt, B.A. Use of bacteriophage T7 RNA polymerase to direct selective high-level expression of cloned genes. *J. Mol. Biol.* **1986**, *189*, 113–130. [[CrossRef](#)]
14. Weickert, M.J.; Doherty, D.H.; Best, E.A.; Olins, P.O. Optimization of heterologous protein production in *Escherichia coli*. *Curr. Opin. Biotechnol.* **1996**, *7*, 494–499. [[CrossRef](#)]
15. Chen, C.W. *Implementation of ICH Q8 and QbD—An FDA Perspective*; International Society for Pharmaceutical Engineering (ISPE): Yokohama, Japan, 2006.
16. ICH Expert Working Group. *Pharmaceutical Development Q8 (R2): ICH Harmonised Tripartite Guideline*; ICH: Geneva, Switzerland, 2009.
17. Beg, S.; Hasnain, M.S.; Rahman, M.; Swain, S. Introduction to Quality by Design (QbD): Fundamentals, Principles, and Applications. In *Pharmaceutical Quality by Design*; Elsevier: Amsterdam, The Netherlands, 2019; pp. 1–17, ISBN 9780128157992.
18. Rathore, A.S.; Winkle, H. Quality by design for biopharmaceuticals. *Nat. Biotechnol.* **2009**, *27*, 26–34. [[CrossRef](#)]
19. Chen, Y.; Yang, O.; Sampat, C.; Bhalode, P.; Ramachandran, R.; Ierapetritou, M. Digital Twins in Pharmaceutical and Biopharmaceutical Manufacturing: A Literature Review. *Processes* **2020**, *8*, 1088. [[CrossRef](#)]
20. Yu, L.X. Pharmaceutical quality by design: Product and process development, understanding, and control. *Pharm. Res.* **2008**, *25*, 781–791. [[CrossRef](#)]
21. Matsunami, K.; Ryckaert, A.; Peeters, M.; Badr, S.; Sugiyama, H.; Nopens, I.; Beer, T.D. Analysis of the Effects of Process Parameters on Start-Up Operation in Continuous Wet Granulation. *Processes* **2021**, *9*, 1502. [[CrossRef](#)]
22. Meitz, A.; Sagmeister, P.; Langemann, T.; Herwig, C. An Integrated Downstream Process Development Strategy along QbD Principles. *Bioengineering* **2014**, *1*, 213–230. [[CrossRef](#)]
23. Schmidt, A.; Helgers, H.; Vetter, F.L.; Juckers, A.; Strube, J. Digital Twin of mRNA-Based SARS-COVID-19 Vaccine Manufacturing towards Autonomous Operation for Improvements in Speed, Scale, Robustness, Flexibility and Real-Time Release Testing. *Processes* **2021**, *9*, 748. [[CrossRef](#)]
24. Lopez, P.C.; Udugama, I.A.; Thomsen, S.T.; Roslander, C.; Junicke, H.; Mauricio-Iglesias, M.; Gernaey, K.V. Towards a digital twin: A hybrid data-driven and mechanistic digital shadow to forecast the evolution of lignocellulosic fermentation. *Biofuels Bioprod. Bioref.* **2020**, *14*, 1046–1060. [[CrossRef](#)]
25. Del Castillo-Romo, A.Á.; Morales-Rodríguez, R.; Román-Martínez, A. Multi-objective optimization for the biotechnological conversion of lingocellulosic biomass to value-added products. In *26th European Symposium on Computer Aided Process Engineering*; Elsevier: Amsterdam, The Netherlands, 2016; pp. 1515–1520, ISBN 9780444634283.
26. Brunef, R.; Kumar, K.S.; Guillen-Gosalbez, G.; Jimenez, L. Integrating process simulation, multi-objective optimization and LCA for the development of sustainable processes. In *21st European Symposium on Computer Aided Process Engineering*; Elsevier: Amsterdam, The Netherlands, 2011; pp. 1271–1275, ISBN 9780444538956.
27. Brunet, R.; Guillén-Gosálbez, G.; Pérez-Correa, J.R.; Caballero, J.A.; Jiménez, L. Hybrid simulation-optimization based approach for the optimal design of single-product biotechnological processes. *Comput. Chem. Eng.* **2012**, *37*, 125–135. [[CrossRef](#)]
28. Udugama, I.A.; Lopez, P.C.; Gargalo, C.L.; Li, X.; Bayer, C.; Gernaey, K.V. Digital Twin in biomanufacturing: Challenges and opportunities towards its implementation. *Syst. Microbiol. Biomanuf.* **2021**, *1*, 257–274. [[CrossRef](#)]
29. Da Costa Basto, R.M.; Casals, M.P.; Mudde, R.F.; van der Wielen, L.A.; Cuellar, M.C. A mechanistic model for oil recovery in a region of high oil droplet concentration from multiphasic fermentations. *Chem. Eng. Sci.* **2019**, *3*, 100033. [[CrossRef](#)]
30. Mat Isham, N.K.; Mokhtar, N.; Fazry, S.; Lim, S.J. The development of an alternative fermentation model system for vinegar production. *LWT* **2019**, *100*, 322–327. [[CrossRef](#)]
31. Pérez, A.D.; van der Bruggen, B.; Fontalvo, J. Modeling of a liquid membrane in Taylor flow integrated with lactic acid fermentation. *Chem. Eng. Process.-Process Intensif.* **2019**, *144*, 107643. [[CrossRef](#)]
32. Udugama, I.; Öner, M.; Lopez, P.C.; Beenfeldt, C.; Bayer, C.; Huusom, J.K.; Gernaey, K.V.; Sin, G. Towards Digitalization in Bio-Manufacturing Operations: A Survey on Application of Big Data and Digital Twin Concepts in Denmark. *Front. Chem. Eng.* **2021**, *3*, 727152. [[CrossRef](#)]
33. Zurdo, J.; Arnell, A.; Obrezanova, O.; Smith, N.; La Gómez de Cuesta, R.; Gallagher, T.R.A.; Michael, R.; Stallwood, Y.; Ekblad, C.; Abrahamsén, L.; et al. Early implementation of QbD in biopharmaceutical development: A practical example. *Biomed Res. Int.* **2015**, *2015*, 605427. [[CrossRef](#)]

34. Pugh, K. Prior Knowledge in Product Development/Design. Available online: https://www.google.com/url?sa=t&rct=j&q=&esrc=s&source=web&cd=&ved=2ahUKewjE5a-Y9vbzAhU0g_0HHSUvCk4QFnoECAoQAQ&url=https%3A%2F%2Fwww.ema.europa.eu%2Fdocuments%2Fpresentation%2Fpresentation-regulators-perspective-session-2-keith-pugh_en.pdf&usg=AOvVaw0NxDIcs8-EMstl-sdm9IxX (accessed on 1 March 2022).
35. Schmidt, A.; Strube, J. Distinct and Quantitative Validation Method for Predictive Process Modeling with Examples of Liquid-Liquid Extraction Processes of Complex Feed Mixtures. *Processes* **2019**, *7*, 298. [[CrossRef](#)]
36. Alt, N.; Zhang, T.Y.; Motchnik, P.; Taticek, R.; Quarmby, V.; Schlothauer, T.; Beck, H.; Emrich, T.; Harris, R.J. Determination of critical quality attributes for monoclonal antibodies using quality by design principles. *Biologicals* **2016**, *44*, 291–305. [[CrossRef](#)]
37. Yu, L.X.; Amidon, G.; Khan, M.A.; Hoag, S.W.; Polli, J.; Raju, G.K.; Woodcock, J. Understanding pharmaceutical quality by design. *AAPS J.* **2014**, *16*, 771–783. [[CrossRef](#)] [[PubMed](#)]
38. Zobel-Roos, S.; Schmidt, A.; Mestmäcker, F.; Mouellef, M.; Huter, M.; Uhlenbrock, L.; Kornecki, M.; Lohmann, L.; Ditz, R.; Strube, J. Accelerating Biologics Manufacturing by Modeling or: Is Approval under the QbD and PAT Approaches Demanded by Authorities Acceptable Without a Digital-Twin? *Processes* **2019**, *7*, 94. [[CrossRef](#)]
39. Kis, Z.; Kontoravdi, C.; Shattock, R.; Shah, N. Resources, Production Scales and Time Required for Producing RNA Vaccines for the Global Pandemic Demand. *Vaccines* **2020**, *9*, 3. [[CrossRef](#)] [[PubMed](#)]
40. Kornecki, M.; Schmidt, A.; Strube, J. PAT as key-enabling technology for QbD in pharmaceutical manufacturing A conceptual review on upstream and downstream processing. *Chim. Oggi-Chem. Today* **2018**, *36*, 44–48.
41. Helgers, H.; Schmidt, A.; Lohmann, L.J.; Vetter, F.L.; Juckers, A.; Jensch, C.; Mouellef, M.; Zobel-Roos, S.; Strube, J. Towards Autonomous Operation by Advanced Process Control—Process Analytical Technology for Continuous Biologics Antibody Manufacturing. *Processes* **2021**, *9*, 172. [[CrossRef](#)]
42. Helgers, H.; Hengelbrock, A.; Schmidt, A.; Rosengarten, J.; Stitz, J.; Strube, J. Process Design and Optimization towards Digital Twins for HIV-Gag VLP Production in HEK293 Cells, including Purification. *Processes* **2022**, *10*, 419. [[CrossRef](#)]
43. Schmidt, A.; Helgers, H.; Vetter, F.L.; Juckers, A.; Strube, J. Fast and Flexible mRNA Vaccine Manufacturing as a Solution to Pandemic Situations by Adopting Chemical Engineering Good Practice—Continuous Autonomous Operation in Stainless Steel Equipment Concepts. *Processes* **2021**, *9*, 1874. [[CrossRef](#)]
44. Helgers, H.; Hengelbrock, A.; Schmidt, A.; Strube, J. Digital Twins for Continuous mRNA Production. *Processes* **2021**, *9*, 1967. [[CrossRef](#)]
45. Woodcock, J. Modernizing Pharmaceutical Manufacturing—Continuous Manufacturing as a Key Enabler: MIT-CMAC International Symposium on Continuous Manufacturing of Pharmaceuticals. Available online: https://iscmp.mit.edu/sites/default/files/documents/ISCMP%202014%20-%20Keynote_Slides.pdf (accessed on 6 December 2021).
46. Grote, F.; Fröhlich, H.; Strube, J. Integration of Ultrafiltration Unit Operations in Biotechnology Process Design. *Chem. Eng. Technol.* **2011**, *34*, 673–687. [[CrossRef](#)]
47. Weisbach, J.L. *Lehrbuch der Ingenieur-und Maschinen-Mechanik: Theoretische Mechanik*; Druck und Verlag von Friedrich Vieweg und Sohn: Braunschweig, Germany, 1845.
48. Darcy, H. *Les Fontaines Publiques de la ville de Dijon: Exposition et Application*; Victor Dalmont: Paris, France, 1856.
49. Brown, G.O. The History of the Darcy-Weisbach Equation for Pipe Flow Resistance. In *Proceedings of the Environmental and Water Resources History, Environmental and Water Resources History Sessions at ASCE Civil Engineering Conference and Exposition 2002, Washington, DC, USA, 3–7 November 2002*; Rogers, J.R., Fredrich, A.J., Eds.; American Society of Civil Engineers: Reston, VA, USA, 2002; pp. 34–43, ISBN 9780784406502.
50. van den Berg, G.B.; Smolders, C.A. Flux decline in ultrafiltration processes. *Desalination* **1990**, *77*, 101–133. [[CrossRef](#)]
51. Wijmans, J.G.; Nakao, S.; van den Berg, J.; Troelstra, F.R.; Smolders, C.A. Hydrodynamic resistance of concentration polarization boundary layers in ultrafiltration. *J. Membr. Sci.* **1985**, *22*, 117–135. [[CrossRef](#)]
52. Huter, M.J.; Strube, J. Model-Based Design and Process Optimization of Continuous Single Pass Tangential Flow Filtration Focusing on Continuous Bioprocessing. *Processes* **2019**, *7*, 317. [[CrossRef](#)]
53. Kumar, A.; Wahlund, P.-O.; Kepka, C.; Galaev, I.Y.; Mattiasson, B. Purification of histidine-tagged single-chain Fv-antibody fragments by metal chelate affinity precipitation using thermoresponsive copolymers. *Biotechnol. Bioeng.* **2003**, *84*, 494–503. [[CrossRef](#)] [[PubMed](#)]
54. Rodrigo, G.; Gruvegård, M.; van Alstine, J. Antibody Fragments and Their Purification by Protein L Affinity Chromatography. *Antibodies* **2015**, *4*, 259–277. [[CrossRef](#)]
55. Sakhnini, L.I.; Pedersen, A.K.; León, I.R.; Greisen, P.J.; Hansen, J.J.; Vester-Christensen, M.B.; Bülow, L.; Dainiak, M.B. Optimizing selectivity of anion hydrophobic multimodal chromatography for purification of a single-chain variable fragment. *Eng. Life Sci.* **2019**, *19*, 490–501. [[CrossRef](#)] [[PubMed](#)]
56. Guiochon, G.; Felinger, A.; Shirazi, D.G.; Katti, A.M. *Fundamentals of Preparative and Nonlinear Chromatography*, 2nd ed.; Elsevier Academic Press: Amsterdam, The Netherlands; Boston, MA, USA; Heidelberg, Germany; London, UK; New York, NY, USA; Oxford, UK; Paris, France; San Diego, CA, USA; San Francisco, CA, USA; Singapore; Sydney, Australia; Tokyo, Japan, 2006; ISBN 9780123705372.
57. Gottesman, S. Proteases and their targets in *Escherichia coli*. *Annu. Rev. Genet.* **1996**, *30*, 465–506. [[CrossRef](#)]

58. Zobel-Roos, S.; Mouellef, M.; Ditz, R.; Strube, J. Distinct and Quantitative Validation Method for Predictive Process Modelling in Preparative Chromatography of Synthetic and Bio-Based Feed Mixtures Following a Quality-by-Design (QbD) Approach. *Processes* **2019**, *7*, 580. [[CrossRef](#)]
59. Zobel-Roos, S. Entwicklung, Modellierung und Validierung von Integrierten Kontinuierlichen Gegenstrom-Chromatographie-Prozessen. Ph.D. Thesis, Shaker Verlag GmbH, Technische Universität Clausthal, Clausthal-Zellerfeld, Germany, 2018.
60. Brooks, C.A.; Cramer, S.M. Steric mass-action ion exchange: Displacement profiles and induced salt gradients. *AIChE J.* **1992**, *38*, 1969–1978. [[CrossRef](#)]
61. Carta, G.; Jungbauer, A. *Protein Chromatography: Process Development and Scale-Up*; Wiley-VCH: Weinheim, Germany, 2010; ISBN 978-3-527-31819-3.
62. Seidel-Morgenstern, A.; Guiochon, G. Modelling of the competitive isotherms and the chromatographic separation of two enantiomers. *Chem. Eng. Sci.* **1993**, *48*, 2787–2797. [[CrossRef](#)]
63. Langmuir, I. the adsorption of gases on plane surfaces of glass, mica and platinum. *J. Am. Chem. Soc.* **1918**, *40*, 1361–1403. [[CrossRef](#)]
64. Seidel-Morgenstern, A. Experimental determination of single solute and competitive adsorption isotherms. *J. Chromatogr. A* **2004**, *1037*, 255–272. [[CrossRef](#)] [[PubMed](#)]
65. Carta, G.; Rodrigues, A.E. Diffusion and convection in chromatographic processes using permeable supports with a bidisperse pore structure. *Chem. Eng. Sci.* **1993**, *48*, 3927–3935. [[CrossRef](#)]
66. Wilson, E.J.; Geankoplis, C.J. Liquid Mass Transfer at Very Low Reynolds Numbers in Packed Beds. *Ind. Eng. Chem. Fund.* **1966**, *5*, 9–14. [[CrossRef](#)]
67. Klepzig, L.S.; Juckers, A.; Knerr, P.; Harms, F.; Strube, J. Digital Twin for Lyophilization by Process Modeling in Manufacturing of Biologics. *Processes* **2020**, *8*, 1325. [[CrossRef](#)]
68. Juckers, A.; Knerr, P.; Harms, F.; Strube, J. Advanced Process Analytical Technology in Combination with Process Modeling for Endpoint and Model Parameter Determination in Lyophilization Process Design and Optimization. *Processes* **2021**, *9*, 1600. [[CrossRef](#)]
69. Martin Christ Gefriertrocknungsanlagen GmbH. Pilot-Gefriertrocknungsanlagen Innovative Technologie. Available online: https://www.martinchrist.de/fileadmin/user_upload/christ/PDF/Broschueren/Pilot/Christ_Pilot_GT_dt_2021-08.pdf (accessed on 22 February 2022).
70. Rambhatla, S.; Pikal, M.J. Heat and mass transfer scale-up issues during freeze-drying, I: Atypical radiation and the edge vial effect. *AAPS PharmSciTech* **2003**, *4*, E14. [[CrossRef](#)]
71. Lindner, R. Prozessentwicklung zur Produktion und Reinigung eines PEGylierten Antikörperfragmentes. Ph.D. Thesis, University of Stuttgart, Stuttgart, Germany, 2019.